IET Electric Power Applications

Research Article

IET Journals
The Institution of Engineering and Technology

Rolling bearing fault detection of electric motor using time domain and frequency domain features extraction and ANFIS

ISSN 1751-8660
Received on 16th January 2018
Revised 17th May 2018
Accepted on 7th June 2018
E-First on 6th February 2019
doi: 10.1049/iet-epa.2018.5274
www.ietdl.org

Hamed Helmi[1] ✉, *Ahmad Forouzantabar*[1]

[1]*Department of Electrical Engineering, Marvdasht Branch, Islamic Azad University, Marvdasht, Fars, Iran*

✉ *E-mail: hamed.helmi@miau.ac.ir*

Abstract: Demands for various products, higher qualities, reduction of costs and competitiveness, have resulted in the use of intelligent fault detection systems. Bearing fault diagnosis as a major component of the electric motors has had an essential role in the operation of production units' reliability. In addition, vibration analysis is one of the most powerful tools in diagnostics. Advances in signal processing technology and electrical equipment have developed a machinery condition monitoring for defect detection. This study has used the extracted features of vibration signals and the adaptive neuro-fuzzy interface system (ANFIS) network proposing a structure for fault detection and diagnosis of rolling bearings. Time-domain and frequency-domain statistical characteristics have been extracted fault information from vibration signals. Besides, the test data sets are presented to the ANFIS network. Simulation results indicated that the performance of the ANFIS network is acceptable. The results reveal that this method has more accuracy and better classification performance in comparison with other methods proposed in the literature.

1 Introduction

Machinery monitoring is of utmost importance in modern industries as it can enhance machines reliability and decrease the loss of production because of damage caused by different defects. Fault diagnosis of rolling element bearings using artificial neural networks (ANNs) [1–4], back-propagation neural network [5, 6], hybrid neural network [7–10], support vector machines [11, 12], wavelet [13, 14] and empirical mode decomposition analysis [15–18] there are methods that provide abundant information about machine faults and have been widely used to detect bearing faults. Rolling bearings being the important components in machinery are extensively used in the electric motors. Faults in the bearings can cause breakdown of the electric motors. Thus, it is important to have the ability to exactly detect and diagnose the severity and existence of the fault happening in the bearing.

Kang *et al.* [19] proposed a novel state assessment method based on the multiple-domain features. Osman and Wang [20] proposed a new morphological Hilbert–Huang (MH) technique for incipient bearing fault detection. Wang and He [21] used a new method, called wavelet packet envelope manifold (WPEM) approach. The WPEM method performs a manifold learning algorithm on a high-dimensional subband envelope feature space without the optimal band selection. The two recent methods are more pre-processing and finding features that fault severity is detected more accurately and have somewhat succeeded.

This paper approaches the use of statistical features of time domain and frequency domain without preprocessing, demodulation, using denoising methods and filtering.

The vibration dataset applied in this paper is acquired from the Case Western Reserve University Rolling Element Bearing Data Center. A tow horsepower (hp) and the three-phase induction motor are jointed to a torque transducer and a dynamometer preferred torque load ranges may be performed with the aid of the dynamometer is controlled. Vibration signals were collected using accelerometers, which were placed in the housing with magnetic bases of the electric motor [22]. As shown in Fig. 1, the test set includes of a three-phase electric motor; a torque converter and a dynamometer.

The data being tested by the motor shaft bearings, SKF 6205 are kept on the drive. Defects with axis rotary engine with speeds of 1730, 1750, 1772 and 1797 RPM were carried out with data received from the dataset of the rolling bearing. Single point faults with fault diameters of 0.007 inches and 0.021 inches and depth of 0.011 inches were inset to the test bearings the use of electro-discharge machining. The load zone is centred at 6 o'clock position. Various types of ball bearing damages are shown in Fig. 2.

All signals were recorded for motor loads of 0–3 hp at a sampling frequency of 48 kHz. In order to test the proposed diagnosis methodology, four sets of data from the experimental system were used: (i) under good conditions; (ii) with a fault on the

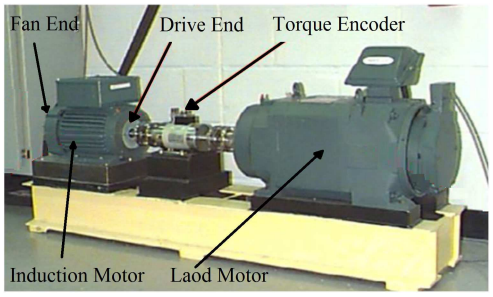

Fig. 1 *Experimental three-phase electric motor*

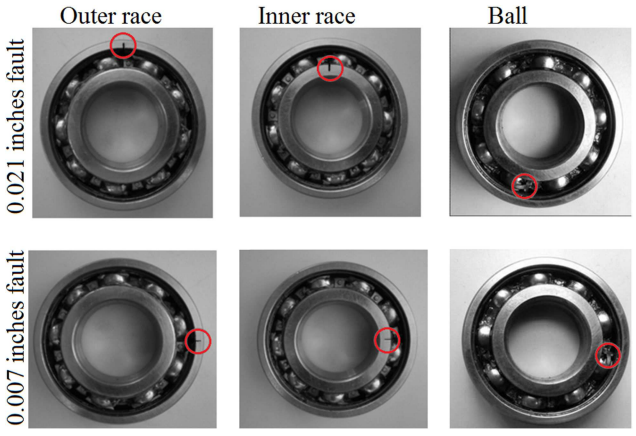

Fig. 2 *Ball bearing the possible defects*

Table 1 Describes the training data and test data for different bearing conditions

Category tags (labels)	Baring condition	Defect, in.	Test data	Training data	RPM	Load, hp
1	healthy	0	12	38	1797	0
			12	38	1772	1
			12	38	1750	2
			12	38	1730	3
2	outer ring fault	0.007	12	38	1797	0
			12	38	1772	1
			12	38	1750	2
			12	38	1730	3
3	inner ring fault	0.007	12	38	1797	0
			12	38	1772	1
			12	38	1750	2
			12	38	1730	3
4	ball fault	0.007	12	38	1797	0
			12	38	1772	1
			12	38	1750	2
			12	38	1730	3
5	outer ring fault	0.021	12	38	1797	0
			12	38	1772	1
			12	38	1750	2
			12	38	1730	3
6	inner ring fault	0.021	12	38	1797	0
			12	38	1772	1
			12	38	1750	2
			12	38	1730	3
7	ball fault	0.021	12	38	1797	0
			12	38	1772	1
			12	38	1750	2
			12	38	1730	3

outer race; (iii) with a fault on the inner race and (iv) with a ball fault. Vibration data details are given in Table 1. According to the table, the vibration dataset are created in seven classes of damage to the rolling bearing (fault severity classification).

It should be noted that the size of the defect or damage is very important in the damaged component because in this particular case the most important part is the inner ring bearing, which ends with the severe damage to the bearing life. Dataset consists of 1400 samples being categorised into two groups of training and testing. There is no one way of choosing the size of training or testing set and applies heuristics such as 10% testing and 90% training. Here is 76% of the data used for training and 24% of the data used for testing. Sample rate represents the number of data points that are sampled within 1 s. Here the vibration signal sample includes 4098 data points and the sampling frequency is 48 kHz. The time for data window is 0.085 s ($T_0 = N * T$), where T is the sampling rate and N is the number of data points. Signal samples from normal and defective rolling bearings are shown in Fig. 3.

1.1 Fast Fourier transform (FFT)

FFT is a mathematical algorithm used to transform a signal from time domain to frequency domain. The spectrum $s(k)$ of a given signal $x(t)$ is defined by where $x(t)$, $s(k)$, and s are the time signal, the frequency signal, and the frequency, respectively, and spectrums of vibration signals of inner race faults and outer race by the application of FFT are presented in Fig. 4

$$s(k) = \int_{-\infty}^{+\infty} x(t) \mathrm{e}^{-\mathrm{j}2\pi kt}\, \mathrm{d}t \tag{1}$$

The initial analysis of the frequency spectrum shows that as the size of the defect increases, the frequency amplitude also increases. However, due to the vibration signals of the ball bearings are non-stationary, the recent rule cannot be generalised in determining the severity and location of the defect.

2 Feature extraction and selection

In this study, the vibration signals of the original dataset contained 4096 data points. For each signal is extracted 15 time-domain features. The fifteen time-domain feature parameters (mean, standard deviation, square mean root, impulse factor, peak value, skewness, kurtosis, crest factor, clarence or margin factor, shape factor, root mean square, mean absolute, standard deviation absolute, skewness absolute, kurtosis absolute) are shown in Table 2, where $x(n)$ is a signal series for $n = 1, 2, \ldots, N$. N is the number of data points.

By evaluating signals of faulty condition with those of the healthy condition through FFT analyser, the analysis is performed with the signal to trace the sidebands of the high frequencies of vibration. The validation is done successfully by taking the input signals from FFT analyser to MATLAB program, being effective for calculating the statistical parameters in faulty condition for frequency-domain analysis.

The frequency domain can disclose the data that cannot be discovered in the time domain. In this work, the frequency spectrums of the vibration signals obtained by FFT for extraction thirteen frequency-domain features (mean, frequency centre, root variance, root mean square, kurtosis, skewness etc.) used as shown in Table 3, where $s(k)$ is a spectrum for $k = 1, 2, \ldots, K$. K is the number of spectrum lines; f_k is the frequency value of the kth spectrum line.

3 Adaptive neuro-fuzzy interface system (ANFIS) network

The ANFIS network represent a fuzzy Takagi–Sugeno–Kang where the fuzzy inference system (FIS) is optimised using the training of ANNs. It was presented by Jang [23]. It's one of the most widely used hybrid intelligent systems and offers the benefits of both neural networks and fuzzy logic. It runs on the given input–output dataset to create a FIS, the membership function (MF) parameters that are adjusted using the backpropagation algorithm,

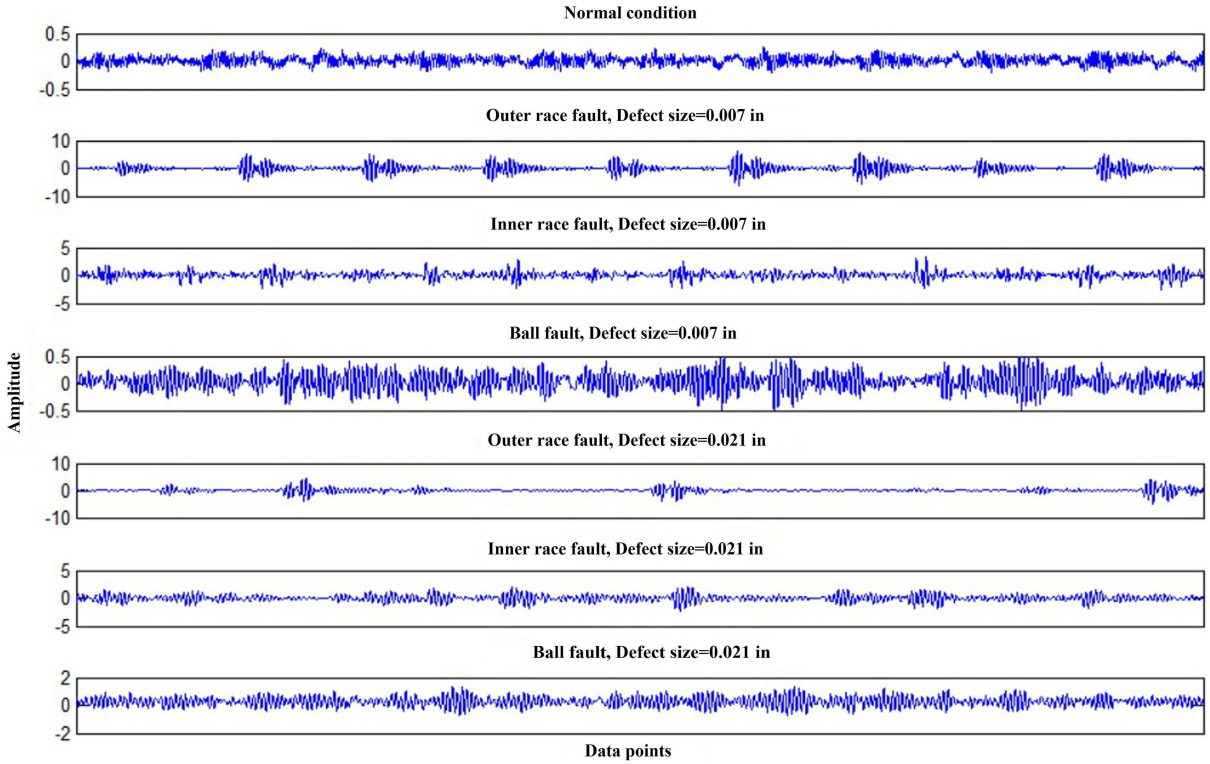

Fig. 3 *Signal samples from normal and defective rolling bearings*

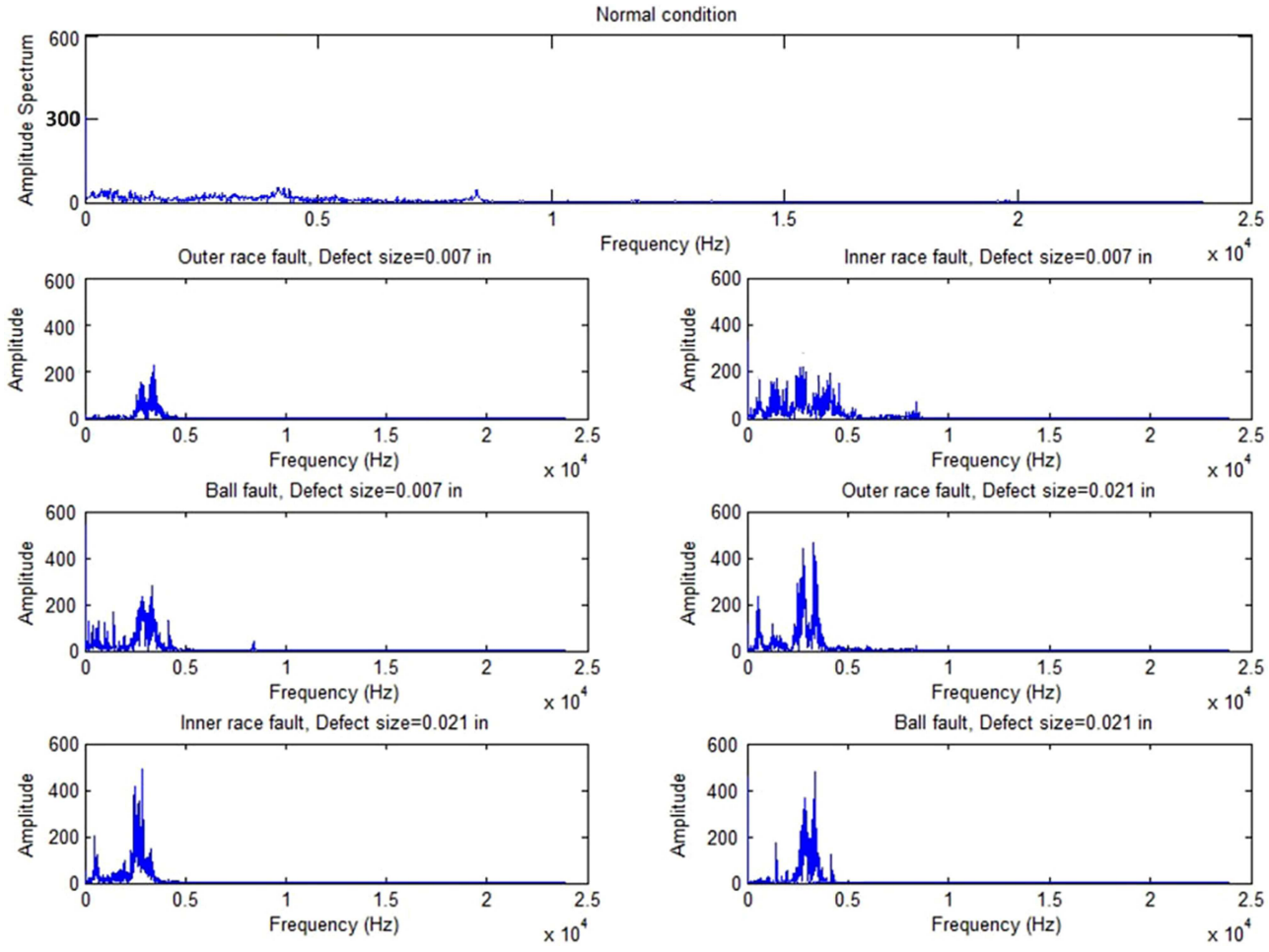

Fig. 4 *Fast Fourier Transformation of vibration signals*

or in combination with a least squares kind of method. This enables the fuzzy system to learn from the data used for the modelling purpose. The neuro-adaptive learning technique in ANFIS is founded the fuzzy modelling procedure is can learn details about the dataset. After that, it computes the parameters of MF that model the given input–output dataset. With regards to fuzzy logic,

Table 2 Features extraction of time domain

$T_1 = \frac{\sum_{n=1}^{N} x(n)}{N}$	mean	(1)
$T_2 = \sqrt{\frac{\sum_{n=1}^{N} (x(n) - T_1)^2}{N-1}}$	standard deviation	(2)
$T_3 = \left(\frac{\sum_{n=1}^{N} \sqrt{\lvert x(n)\rvert}}{N}\right)^2$	square mean Root	(3)
$T_4 = \sqrt{\frac{\sum_{n=1}^{N} (x(n))^2}{N}}$	root mean square	(4)
$T_5 = \max \lvert x(n)\rvert$	peak value	(5)
$T_6 = \frac{\sum_{n=1}^{N} (x(n) - T_1)^3}{(N-1)T_2^3}$	Skewness	(6)
$T_7 = \frac{\sum_{n=1}^{N} (x(n) - T_1)^4}{(N-1)T_2^4}$	Kurtosis	(7)
$T_8 = \frac{T_5}{T_4}$	Crest factor	(8)
$T_9 = \frac{T_5}{T_3}$	Clarence or margin factor	(9)
$T_{10} = \frac{T_4}{(1/N)\sum_{n=1}^{N} \lvert x(n)\rvert}$	shape factor	(10)
$T_{11} = \frac{T_5}{(1/N)\sum_{n=1}^{N} \lvert x(n)\rvert}$	impulse factor	(11)
$T_{12} = \frac{\sum_{n=1}^{N} \lvert x(n)\rvert}{N}$	mean absolute	(12)
$T_{13} = \sqrt{\frac{\sum_{n=1}^{N} (\lvert x(n)\rvert - T_1)^2}{N-1}}$	standard deviation absolute	(13)
$T_{14} = \frac{\sum_{n=1}^{N} (\lvert x(n)\rvert - T_1)^3}{(N-1)T_2^3}$	skewness absolute	(14)
$T_{15} = \frac{\sum_{n=1}^{N} (\lvert x(n)\rvert - T_1)^4}{(N-1)T_2^4}$	kurtosis absolute	(15)

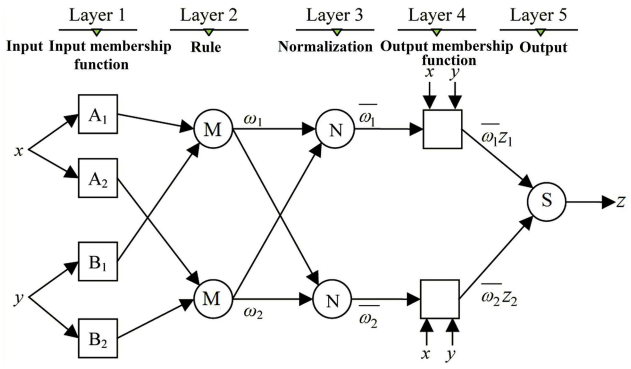

Fig. 5 *ANFIS architecture*

it offers a mapping feature between inputs and outputs. The mapping process is accomplished by using MFs of the input and its associated parameters in relation to the MFs of the output. It's used to complete adjustment of fuzzy logic MFs in combination with the ANN learning feature [23, 24].

A first-order Sugeno FIS are considered, that contains two rules:

Rule 1: If x is A_1 and y is B_1 then $z_1 = p_1x + q_1y + r_1$,
Rule 2: If x is A_2 and y is B_2 then $z_2 = p_2x + q_2y + r_2$,

where A_i and B_i are fuzzy sets, x and y are the inputs, $z_i(i = 1, 2)$ is the output within the fuzzy region. p_i, q_i and r_i are the design parameters which are determined during the training process. ANFIS architecture is shown in Fig. 5. The layers and nodes functions are illustrated.

Table 3 Features extraction of frequency domain

$F_1 = \frac{\sum_{k=1}^{K} s(k)}{K}$	mean	(1)
$F_2 = \frac{\sum_{k=1}^{K} (s(k) - F_1)^2}{K-1}$	variance of mean frequency	(2)
$F_3 = \frac{\sum_{k=1}^{K} (s(k) - F_1)^3}{K(\sqrt{F_2})^3}$	skewness power spectrum	(3)
$F_4 = \frac{\sum_{k=1}^{K} (s(k) - F_1)^4}{KF_2^2}$	kurtosis power spectrum	(4)
$F_5 = \frac{\sum_{k=1}^{K} f_k s(k)}{\sum_{k=1}^{K} s(k)}$	frequency centre	(5)
$F_6 = \sqrt{\frac{\sum_{k=1}^{K} (f_k - F_5)^2 s(k)}{K}}$	root variance	(6)
$F_7 = \sqrt{\frac{\sum_{k=1}^{K} f_k^2 s(k)}{\sum_{k=1}^{K} s(k)}}$	root mean square	(7)
$F_8 = \sqrt{\frac{\sum_{k=1}^{K} f_k^4 s(k)}{\sum_{k=1}^{K} f_k^2 s(k)}}$	mean frequency that crosses the mean of the time-domain signal	(8)
$F_9 = \frac{\sum_{k=1}^{K} f_k^2 s(k)}{\sqrt{\sum_{k=1}^{K} s(k) \sum_{k=1}^{K} f_k^4 s(k)}}$	stabilisation factor	(9)
$F_{10} = \frac{F_6}{F_5}$	coefficient of variability	(10)
$F_{11} = \frac{\sum_{k=1}^{K} (f_k - F_5)^3 s(k)}{KF_6^3}$	skewness	(11)
$F_{12} = \frac{\sum_{k=1}^{K} (f_k - F_5)^4 s(k)}{KF_6^4}$.	kurtosis	(12)
$F_{13} = \frac{\sum_{k=1}^{K} (f_k - F_5)^{1/2} s(k)}{K\sqrt{F_6}}$	root mean square ratio	(13)

3.1 Input MF layer

Each node i in this layer is an adaptive node with a node function. Therefore O_i^1 is the membership grade of a fuzzy set (A_1, A_2, B_1, B_2)

$$O_i^1 = \mu_{Ai}(x), \quad i = 1, 2. \tag{2}$$

$$O_i^1 = \mu_{Bi-2}(x), \quad i = 3, 4. \tag{3}$$

$\mu_{Ai}(x)$ and $\mu_{Bi-2}(x)$ are the fuzzy MFs. The chosen model of the MFs is normally bell-shaped with a maximum extend to one and a minimum extend to zero and is given by

$$\mu_{Ai}(x) = \frac{1}{1 + \left[((x - c_i)/a_i)^2\right]^{b_i}}, \quad i = 1, 2. \tag{4}$$

where a_i, b_i and c_i are the parameters set.

3.2 Rule layer

Each node in this layer is just a fixed node labelled with M. The output is the product of all the incoming signals. The outputs represent the firing strengths ω_i of each rule as

$$O_i^2 = \omega_i = \mu_{Ai}(x) \cdot \mu_{Bi}(y), \quad i = 1, 2. \tag{5}$$

3.3 Normalisation layer

Each node in this layer is just a fixed node labelled with N. The ith node calculates the ratio of the ith rule's firing strength to the sum of all rule's firing strengths and is given as

$$\sum_{i=1}^{2} \omega_i, \quad i = 1, 2. \tag{6}$$

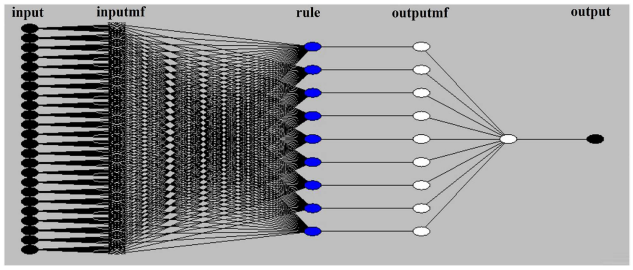

Fig. 6 *ANFIS model*

The outputs are called normalised firing strengths

$$O_i^3 = \overline{\omega_i} = \frac{\omega_i}{\sum_{i=1}^{2} \omega_i}, \quad i = 1, 2. \tag{7}$$

3.4 Output MF layer

Each node i in this layer is definitely an adaptive node with a node function

$$O_i^4 = \overline{\omega_i} z_i = \overline{\omega_i}(p_i x + q_i y + r_i), \quad i = 1, 2. \tag{8}$$

q_i, r_i and p_i are the parameters set of this node.

3.5 Output layer

The single node in this layer is a fixed node labelled S, which computes the entire output while the summation of most inbound signals

$$O_i^5 = z = \sum_{i=1}^{2} \overline{\omega_i} z_i = \frac{\sum_{i=1}^{2} \omega_i z_i}{\sum_{i=1}^{2} \omega_i}. \tag{9}$$

The algorithm used is a combination of the gradient descent method and least squares estimation that comprises two stages to be able to better training efficiency and eliminate possible trapping as a result of local minima. In the prime stage, the assumption parameters are supposed to be fixed. The suitable resultant parameters are then acquired utilising the least squares estimate. In the next stage, the resultant parameters are supposed to be fixed. The assumption parameters are then updated utilising the back-propagation gradient descent approach, on the basis of the error values [24].

According to Table 1, 1068 signals are related to the training dataset and 336 signals are related to the test dataset. The number of training data was selected based on the best network performance during training. Two features of matrices with the sizes of 28*336 and 28*1068 are regarded for the training dataset and test dataset being used as input for the classifier. In this study, 15 time characteristics and 13 frequency characteristics were extracted for the bearing fault diagnosis. In relation to the time signal feature extraction, $x(n)$ is a signal series for $n = 1,2, \ldots, N$, where $N = 4096$ is the number of data points. Time-domain features and frequency-domain features vector are as follows:

$$\boldsymbol{F} = \{T_1,\ T_2,\ T_3,\ T_4,\ T_5,\ T_6,\ T_7, T_8,\ T_9,\ T_{10},\ T_{11}T_{12},\ T_{13},\ T_{14},\ T_{15},\ F_1,\ F_2,\ F_3,\ F_4, F_5,\ F_6,\ F_7,\ F_8,\ F_9,\ F_{10},\ F_{11},\ F_{12}, F_{13}\} \tag{10}$$

4 Fault detection

Fuzzy c-means (FCM) clustering is given separate sets of input and output data and GENFIS3 generates a FIS using FCM clustering [25, 26]. GENFIS3 does this by extracting a set of rules modelling the data behaviour. The FCM clustering function uses the rule extraction method to determine the number of rules and MFs for the antecedents and consequences. The output data from each of the above-specified generation methods will be processed using ANFIS algorithm. ANFIS adaptive neuro-fuzzy is trained by Sugeno-type FIS. ANFIS network uses a hybrid learning algorithm to detect the single-output MF parameters; Sugeno-type inferences fuzzy systems (FIS). ANFIS network uses a hybrid learning algorithm to generate a single-output Sugeno type inferences fuzzy systems (FIS). A combination of BP and least-squares gradient decent methods may be used for training FIS (Sugeno-type FIS) MF parameters to model a given set of input/output data. Finally, the processed output from the ANFIS algorithm has been used to obtain the graphical output. To achieve the ANFIS function, nine fuzzy sets were created. A number of sets defines network rules. The ANFIS' nine rules are described here. Fuzzy MFs are of the Gaussian type. The structure of ANFIS, which includes 24 inputs, one output, and 9 rules, can be seen in Fig. 6.

The parameters of MFs have been adjusted and the ANFIS network trained. Fig. 7 shows the MFs after training the network. Number 9 of the MFs is related to inputs' action. As described, vector input including 28 features is extracted from the signal. Fig. 7 describes a horizontal axis and the vertical axis showing the values of signal characteristics and value of the membership.

5 Results ANFIS network

In Fig. 8, output of the ANFIS network under training is compared with the desired output (target). In Fig. 9, output of the ANFIS network under test is compared with the desired output (target). In Figs. 8 and 9, the absolute error is shown for fault detection, so the ANFIS network's results are marked with a red circle.

Tables 4 and 5, respectively, confusion matrices of the training data and test data are presented for comparison, output data and target data. ANFIS network's performance or accuracy is the number of correctly classified diagnoses divided by the total number of diagnoses. ANFIS network's performance of training and test datasets is 99.2 and 98.2%, respectively. Thus, the proposed method shows a good performance. Healthy mode (label 1) has been fully recognised. None of the failure modes has been diagnosed as healthy. This issue is very important in practical applications since the proposed method is diagnosed as a 100% healthy being important in planned maintenance and replacement parts, as well.

In a statistical analysis of classification, the F-score is a measure of a test's accuracy. It considers both the precision p and the recall r of the test to compute the score: p is the number of correct positive results divided by the number of all positive results returned by the classifier, and r is the number of correct positive results divided by the number of all relevant samples. In general, positive = identified and negative = rejected. Therefore

- true positive = correctly identified,
- false positive = incorrectly identified,
- true negative = correctly rejected,
- false negative = incorrectly rejected (Fig. 10).

The equations are shown as follows:

$$\text{Accuracy} = \frac{\text{TP} + \text{TN}}{\text{TP} + \text{TN} + \text{FP} + \text{FN}} \tag{11}$$

$$\text{Precision} = \frac{\text{TP}}{\text{TP} + \text{FP}} \tag{12}$$

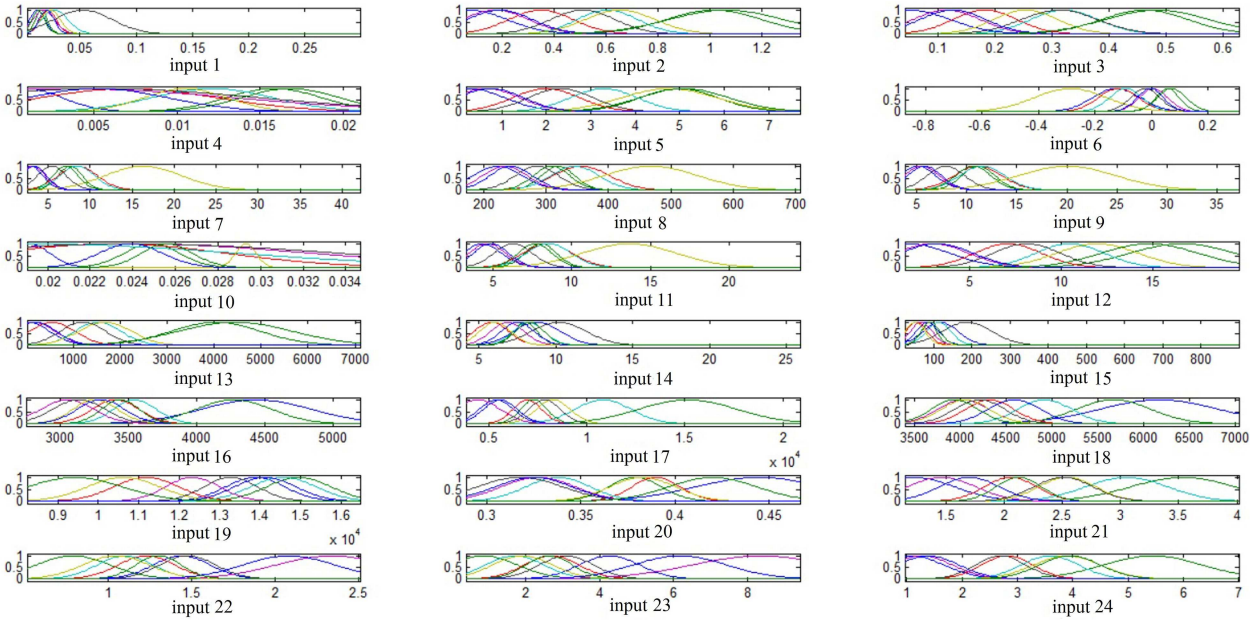

Fig. 7 *MFs for each input feature after training. The vertical axis represents the degree of membership*

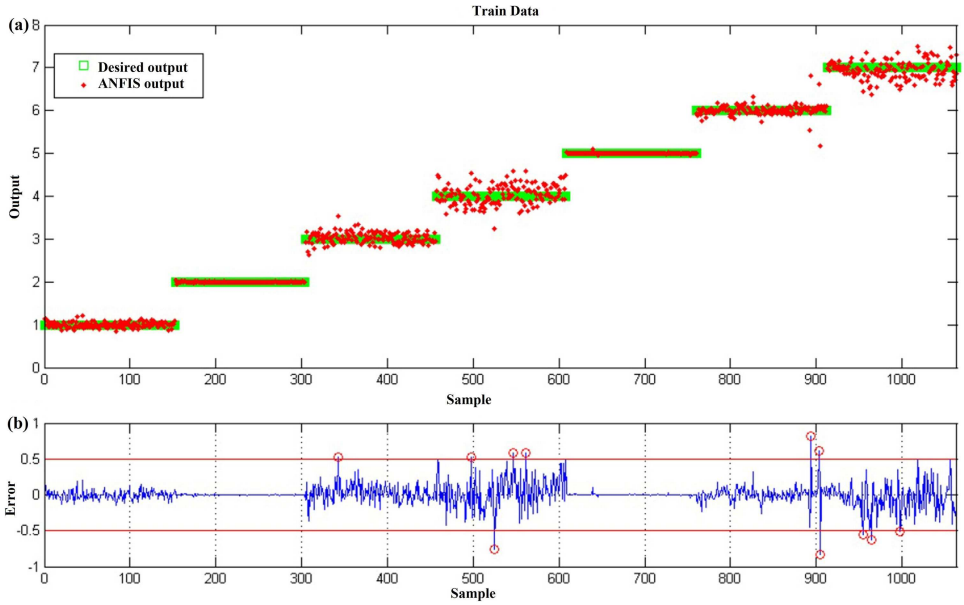

Fig. 8 *Results of classification using feature extraction time and frequency characteristics of the training dataset*
(a) ANFIS output ***(b)*** ANFIS error in prediction output compared with the results desired(target)

$$\text{Recall or Sensitivity} = \frac{\text{TP}}{\text{TP} + \text{FN}} \tag{13}$$

$$\text{Specificity} = \frac{\text{TN}}{\text{TN} + \text{FP}} \tag{14}$$

$$F-\text{score} = \frac{2 * \text{TP}}{2 * \text{TP} + \text{FP} + \text{FN}} \tag{15}$$

In Table 6, accuracy, precision, recall, specificity and *F*-score are calculated for confusion matrix of ANFIS under test data.

In Table 7, the proposed method is compared with previous studies. The results reveal that this method has more accuracy and better classification performance in comparison with other methods proposed in the literature.

6 Conclusion

In this paper, a method to rolling bearing fault detection of the electric motor using time-domain and frequency-domain features extraction and ANFIS is proposed based on statistics analysis and adaptive neuro-FIS. Defect information acquired from the vibration signals where time-domain and frequency-domain statistical characteristics are extracted. ANFIS network trained the test datasets being presented to the network. Results indicate that the performance of the ANFIS is acceptable.

The efficiency of ANFIS is 98%. The results indicate that the proposed method enables the detection of faults in bearings and concurrent identification of the severity and category of faults with a high accuracy.

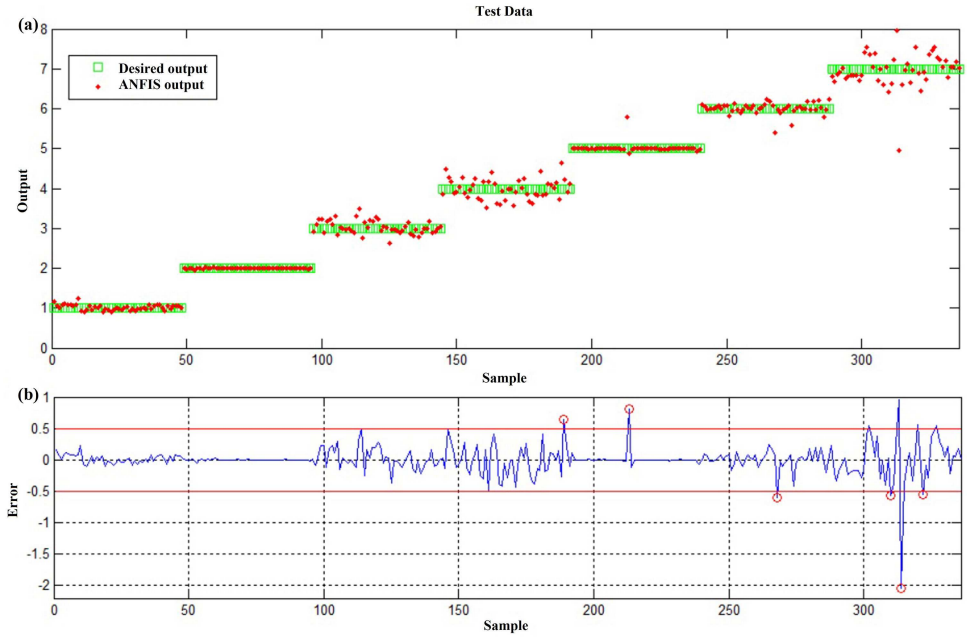

Fig. 9 *Results of classification using feature extraction time and frequency characteristics of the test dataset*
(a) ANFIS output, ***(b)*** ANFIS error in prediction output compared with the results desired(target)

Table 4 Confusion matrix of ANFIS on training data

		Target						
ANFIS output	label	1	2	3	4	5	6	7
	1	152	0	0	0	0	0	0
	2	0	152	0	0	0	0	0
	3	0	0	151	1	0	0	0
	4	0	0	1	148	0	0	0
	5	0	0	0	3	152	1	0
	6	0	0	0	0	0	149	3
	7	0	0	0	0	0	2	149

Table 5 Confusion matrix of ANFIS on test data

		Target						
ANFIS output	Label	1	2	3	4	5	6	7
	1	48	0	0	0	0	0	0
	2	0	48	0	0	0	0	0
	3	0	0	48	0	0	0	0
	4	0	0	0	47	0	0	0
	5	0	0	0	1	47	1	1
	6	0	0	0	0	1	47	2
	7	0	0	0	0	0	0	45

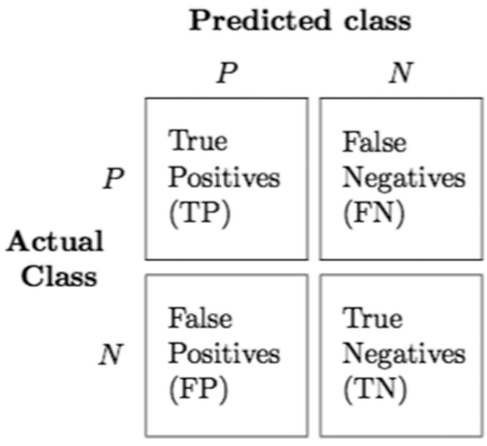

Fig. 10 *Confusion matrix*

Table 6 F-score and precision confusion matrix of ANFIS on test data

	Class						
—	1	2	3	4	5	6	7
TP	48	48	48	47	47	47	45
TN	282	282	282	283	283	283	285
FP	0	0	0	0	3	3	0
FN	0	0	0	1	1	1	3
accuracy	1	1	1	0.99	0.98	0.98	0.99
precision	1	1	1	0.97	0.97	0.97	0.93
recall	1	1	1	1	0.94	0.94	1
specificity	1	1	1	0.99	0.99	0.99	0.98
F-score	1	1	1	0.98	0.95	0.95	0.96

Table 7 Comparison of the proposed method with the methods in the literature

Reference	Method	Accuracy, %	Fault types	Training and testing samples
[5]	ANN	93	4	144
[9]	hidden Markov model	92	4	36
[12]	support vector machine	90	2	135
[19]	relative compensation distance of multiple-domain features	95	10	4850
adaptive neural-based FIS of the proposed approach		98	7	1400

7 References

[1] Kazlas, P.T., Monsen, P.T., LeBlanc, M.J.: 'Neural network-based helicopter gearbox health monitoring system'. Neural Networks for Processing [1993] III, Proc. the 1993 IEEE-SP Workshop, Maryland, USA, 1993, pp. 431–440

[2] Samanta, B., Al-Balushi, K.R.: 'Artificial neural network based fault diagnostics of rolling element bearings using time-domain features', *Mech. Syst. Signal Process.* ., 2003, **17**, (2), pp. 317–328

[3] Kalkat, M, Yildirim, Ş., Uzmay, I.: 'Design of artificial neural networks for rotor dynamics analysis of rotating machine systems', *Mechatronics. (Oxf)*, 2005, **15**, (5), pp. 573–588

[4] Wang, C.C., Kang, Y., Shen, P.C*., et al.*: 'Applications of fault diagnosis in rotating machinery by using time series analysis with neural network', *Expert Syst. Appl.*, 2010, **37**, (2), pp. 1696–1702

[5] Li, B., Chow, M.Y., Tipsuwan, Y*., et al.*: 'Neural-network-based motor rolling bearing fault diagnosis', *IEEE Trans. Ind. Electron.*, 2000, **47**, (5), pp. 1060–1069

[6] Dou, D., Yang, J., Liu, J*., et al.*: 'A rule-based intelligent method for fault diagnosis of rotating machinery', *Knowl.-Based Syst.*, 2012, **36**, pp. 1–8

[7] Matsuura, T.: 'An application of neural network for selecting feature parameters in machinery diagnosis', *J. Mater. Process. Technol.*, 2004, **157**, pp. 203–207

[8] Yang, D.M., Stronach, A.F., MacConnell, P*., et al.*: 'Third-order spectral techniques for the diagnosis of motor bearing condition using artificial neural networks', *Mech. Syst. Signal Process.*, 2002, **16**, (2–3), pp. 391–411

[9] Saxena, A., Saad, A.: 'Evolving an artificial neural network classifier for condition monitoring of rotating mechanical systems', *Appl. Soft Comput.*, 2007, **7**, (1), pp. 441–454

[10] Shi, S., Zhang, L., Liang, W.: 'Condition monitoring and fault diagnosis of rolling element bearings based on wavelet energy entropy and SOM'. 2012 Int. Conf. Quality, Reliability, Risk, Maintenance, and Safety Engineering (ICQR2MSE), 2012, pp. 651–655

[11] FernáNdez-Francos, D., MartíNez-Rego, D., Fontenla-Romero, O*., et al.*: 'Automatic bearing fault diagnosis based on one-class ν-SVM', *Comput. Ind. Eng.*, 2013, **64**, (1), pp. 357–365

[12] Samanta, B., Al-Balushi, K.R., Al-Araimi, S.A.: 'Artificial neural networks and support vector machines with genetic algorithm for bearing fault detection', *Eng. Appl. Artif. Intell.*, 2003, **16**, (7), pp. 657–665

[13] Sanz, J., Perera, R., Huerta, C.: 'Fault diagnosis of rotating machinery based on auto-associative neural networks and wavelet transforms', *J. Sound Vib.*, 2007, **302**, (4), pp. 981–999

[14] Rafiee, J., Rafiee, M.A., Tse, P.W.: 'Application of mother wavelet functions for automatic gear and bearing fault diagnosis', *Expert Syst. Appl.*, 2010, **37**, (6), pp. 4568–4579

[15] Lei, Y., Lin, J., He, Z*., et al.*: 'A review on empirical mode decomposition in fault diagnosis of rotating machinery', *Mech. Syst. Signal Process.*, 2013, **35**, (1), pp. 108–126

[16] Huang, P., Pan, Z., Qi, X*., et al.*: 'Bearing fault diagnosis based on EMD and PSD'. 2010 8th World Congress on Intelligent Control and Automation (WCICA), 2010, pp. 1300–1304

[17] Jiang, L., Zhang, Y., Gong, G*., et al.*: 'Fault diagnosis for rolling element bearing using EMD-DFDA'. The 26th Chinese Control and Decision Conf. (2014 CCDC), 2014, pp. 3212–3216

[18] Lei, Y., He, Z., Zi, Y.: 'A new approach to intelligent fault diagnosis of rotating machinery', *Expert Syst. Appl.*, 2008, **35**, (4), pp. 1593–1600

[19] Kang, S., Ma, D., Wang, Y*., et al.*: 'Method of assessing the state of a rolling bearing based on the relative compensation distance of multiple-domain features and locally linear embedding', *Mech. Syst. Signal Process.*, 2017, **86**, pp. 40–57

[20] Osman, S., Wang, W.: 'A morphological Hilbert-Huang transform technique for bearing fault detection', *IEEE Trans. Instrum. Meas.*, 2016, **65**, (11), pp. 2646–2656

[21] Wang, J., He, Q.: 'Wavelet packet envelope manifold for fault diagnosis of rolling element bearings', *IEEE Trans. Instrum. Meas.*, 2016, **65**, (11), pp. 2515–2526

[22] Loparo, K.A.: '*Bearings vibration data set*' (Case Western Reserve University, Cleveland, Ohio, USA, 2008)

[23] Jang, J.S.: 'ANFIS: adaptive-network-based fuzzy inference system', *IEEE Trans. Syst. Man Cybern.*, 1993, **23**, (3), pp. 665–685

[24] Latuny, J.: 'A sensitivity comparison of neuro-fuzzy feature extraction methods from bearing failure signals'. PhD dissertation, Curtin University, 2013

[25] Dunn, J.C.: 'A fuzzy relative of the ISODATA process and its use in detecting compact well-separated clusters', 1973, pp. 32–57

[26] Bezdek, J.C.: '*Pattern recognition with fuzzy objective function algorithms*' (Plenum Press, New York, 1987)